Progranulin Associates With Rab2 and Is Involved in Autophagosome-Lysosome Fusion in Gaucher Disease

Xiangli Zhao
New York University Medical Center
Rossella Liberti
New York University Medical Center
Jinlong Jian
New York University Medical Center
Wenyu Fu
New York University Medical Center
Aubryanna Hettinghouse
New York University Medical Center
Ying Sun
University of Cincinnati College of Medicine
Chuan-ju Liu (chuanju.liu@nyumc.org)
New York University Medical Center https://orcid.org/0000-0002-7181-8032

Research Article

Keywords: Autophagosome-lysosome fusion, Gaucher disease, Progranulin, autophagy, Rab2

Posted Date: May 7th, 2021

DOI: https://doi.org/10.21203/rs.3.rs-457451/v1

Abstract

Progranulin (PGRN) is a key regulator of lysosome and its deficiency has been linked to various lysosomal storage diseases (LSDs), including Gaucher disease (GD), one of the most common LSD. Here, we report that PGRN plays a previously unrecognized role in autophagy within the context of GD. PGRN deficiency associated with accumulation of LC3-II and p62 in autophagosomes of GD animal model and patient fibroblasts, resulting from impaired fusion of autophagosomes and lysosomes. PGRN physically interacted with Rab2, a critical molecule in autophagosome-lysosome fusion. Additionally, a fragment of PGRN containing the Grn E domain was required and sufficient for binding to Rab2. Further, this fragment significantly ameliorated PGRN-deficiency associated impairment of autophagosome-lysosome fusion and autophagic flux. These findings not only demonstrate that PGRN is a crucial mediator of autophagosome-lysosome fusion, but also provide new evidence indicating PGRN's candidacy as a molecular target for modulating autophagy in GD and other LSDs in general.

Key Message

1) PGRN acts as a crucial factor involved in autophagosome-lysosome fusion in GD.

2) PGRN physically interacts with Rab2, a molecule in autophagosome-lysosome fusion.

3) A 15-kDa C-terminal fragment of PGRN is required and sufficient for binding to Rab2.

4) This PGRN derivative ameliorates PGRN-deficiency associated impairment of autophagy.

5) This study provides new insights into autophagy and may develop novel therapy for GD.

Introduction

The autophagy-lysosomal system is responsible for catabolic, degradative processing of unwanted materials and is crucial to the maintenance of cellular and tissue homeostasis. Autophagy-lysosomal processing occurs in several stages; successful progression through these stages depends on integrated function of lysosomes and autophagosomes [1]. Therefore, it is not unexpected that autophagic dysfunction is a prominent feature of several lysosomal storage disorders [2-4]. Gaucher disease (GD), one of the most common genetic lysosomal storage disease (LSD), is caused by mutations in the β-glucocerebrosidase (GCase or *GBA1*) encoding *GBA1* gene, which consequently lead to the accumulation of β-glucosylceramide (β-GlcCer) in macrophages and other cell types [5-7]. Accumulation of β-GlcCer leads to lysosomal dysfunction and subsequent defects in autophagy [3, 8]. Several studies have reported observations of autophagy-lysosomal system impairment in the neuronopathic GD mouse model [3, 9]. Moreover, *GBA1* mutations can also trigger mitochondrial dysfunction and mitophagy defects [10, 11].

Progranulin (PGRN) is a widely expressed glycoprotein linked to a variety of physiologic and disease processes, including early embryogenesis, wound healing, host defense, autoimmune disease, and cancer [12-18]. PGRN exerts its pleiotropic functionality through multiple mechanisms. As a neurotrophic factor, mutations in the *PGRN* gene associate with some neuropathic diseases, such as frontotemporal dementia (FTD) and neuronal ceroid lipofuscinosis (NCL) [19-23]. PGRN also imparts anti-inflammatory effects in various conditions through targeting to TNF receptors [24-27]. Recent reports further reveal an emergent link between PGRN and autophagy, however, the exact mechanism of how PGRN regulates the autophagic pathway is unclear and controversial. PGRN deficient neurons display reduced autophagic flux and enhanced accumulation of pathological forms of TDP-43 [28]. In murine models, PGRN treatment may contribute to adipose insulin resistance via increased autophagy or autophagic imbalance [29, 30], whereas some other reports indicate a controversial effect of PGRN with a reduction in hepatic insulin signaling and autophagy [31].

Recent studies from several laboratories, including ours, have revealed associations between PGRN deficiency and lysosomal storage diseases, such as GD and Tay-Sachs disease [32, 33]. Jian et al. recently reported that PGRN was a co-chaperone for lysosomal localization of GCase through linking GCase to heat shock protein 70 (Hsp70) [14]. Given that impairment of the autophagy pathway is a feature of GD pathology and PGRN is a novel important regulator of autophagosomes [9, 10, 28, 34], we set out to investigate the role of PGRN in autophagy, particularly in PGRN deficiency associated GD. In this study, we found that PGRN interacted with Rab2 and its deficiency impaired the fusion of autophagosomes and lysosomes. More importantly, an approximately 15-kDa PGRN-derived protein, ND7, which was resiposible for binding to Rab2, could effectively ameliorate the impaired autophagosome-lysosome fusion.

Materials And Methods

Reagents and materials

Fibroblasts from Type 2 GD patients were purchased from Coriell Cell Repositories (Camden, NJ). Antibodies against ATG5 (sc-133158), p62/SQSTM1 (sc-28359), LIMP2 (sc-55571), His-tag (sc-57598), GFP (sc-9996), and GAPDH (sc-25778) were purchased from Santa Cruz Biotechnology (Dallas, Texas, USA). Antibody against PCDGF (40-3400) was purchased from Invitrogen (Waltham, MA, USA). Antibody against LC3B (#2775S) was purchased from Cell Signaling Technology (Danvers, MA, USA). Antibodies against Rab2 (ab154729) and Bcl2-L13 (ab25895) were purchased from Abcam (Cambridge, UK). Fluorescence labeled secondary antibodies were purchased from Jackson ImmunoResearch Laboratories, Inc. (West Grove, PA, USA). 4-Methylumbelliferyl β-D-glucopyranoside (4-MUG, Cat. No. M3633) was purchased from Sigma-Aldrich (Natick, MA, USA). LysoTracker Red DND99 (Cat. No. L7528), HisPur™ Ni-NTA Resin (88221), and Pierce High-Capacity Endotoxin Removal Resin (Pub. Part No. 2162373.3) were purchased from Thermo Fisher Scientific (Bridgewater, NJ, USA). DAPI (Cat. No. H-1200) was purchased from VECTOR Laboratories (Burlingame, CA, USA). The plasmid FUW mCherry-GFP-LC3 (#110060) was purchased from Addgene (Watertown, MA, USA). Recombinant His-tag PGRN protein was

purified from Hek293T stable cell lines as described previously [14]. Dulbecco's Modified Eagle Medium (DMEM; Cat. No. 11965–118) and fetal bovine serum (FBS; Cat. No. 16000–044) were purchased from Gibco-BRL (Waltham, MA, USA).

PGRN deficient GD model

All animal experiments were approved by Institutional Animal Care and Use Committee (IACUC) of New York University School of Medicine. Mice were group housed within the rodent barrier facility at the Skirball Institute of Biomolecular Medicine with ad libitum access to food and water in a specific pathogen free room under controlled temperature and humidity on a 12 hour light/dark cycle. C57BL6/J background wild-type (WT) and PGRN KO mice were acquired from Jackson Laboratory and lines were maintained within the animal housing facility. 8 week-old mice were induced with chronic lung inflammation by intraperitoneal (I.P.) injection of Ovalbumin (OVA)-Alum at Day 1 and Day 15, followed by intranasal challenge with 1% OVA, beginning at Day 29 and administered at a frequency of every three days for four weeks. In PGRN and ND7 rescue experiments, the frequency of intranasal challenge with OVA was increased to three times a week, 4 mg/kg/week recombinant PGRN or ND7 were I.P. injected starting from the first week of the intranasal challenge until to the end of this experiment and another group of mice were treated with PBS as a negative control. The mice were sacrificed, and spleen, liver, leg, lung, and bronchoalveolar lavage (BAL) were collected.

Cell culture

GD L444P patient fibroblasts, HEK293T and C28i2 cells were cultured in Dulbecco's modified Eagle's medium (DMEM) supplemented with 10% fetal bovine serum and 1% penicillin-streptomycin.

Generation knockout cell lines for PGRN or Rab2

CRISPR-Cas9 technology was used to delete PGRN or Rab2 genes. The gRNA that targets human PGRN or Rab2 genomic sequence was subcloned into the lentiCRISPR lentiviral plasmid (Addgene, 49535; deposited by Dr. Feng Zhang) following the manufacturer's instruction. For the preparation of lentivirus, human PGRN gRNA or Rab2 gRNA subcloned lentiCRISPR plasmids were cotransfected with lentiviral packaging plasmids (psPAX2 and pMD2.G plasmid) into the HEK293T cells, respectively. 48 h post-transfection, supernatants containing indicated lentivirus particles from cells were harvested. L444P fibroblasts were then infected with the indicated lentivirus and then selected with 1 μg/ml of puromycin for 5-7 days. The PGRN or Rab2 knockout efficiency in these selected cells was analyzed by western blotting.

Western blotting

Protein samples were separated by SDS-PAGE. The samples were transferred to a nitrocellulose membrane after gel electrophoresis. Nonspecific binding was blocked with 5% non-fat milk for 1hr and the membrane was probed with the primary antibody overnight at 4°C. The membrane was washed in 3

five minute washes with TBST prior to incubation with the secondary antibody for 2 hours at room temperature and repeated washing. The bands were developed on the film using ECL Prime Western Blotting Detection Reagent (Amersham Pittsburgh, PA, USA).

Preparation of lipid extraction

Mouse brain tissue was used as a source of lipid mixture. Briefly, one mouse brain was dissected under sterile conditions. The brain tissues were homogenized in 50 ml PBS. Bicinchoninic acid assay was used to determine the protein level in the brain lysate.

LysoTracker assay

Type 2 GD L444P patient fibroblasts were cultured on Black-clear bottom 96-well microplate or coverslips in 24-well plates, and challenged with lipid lysis (50 μg/ml) for 24 h. The next day, fresh medium containing 300 nM LysoTracker® Red was added for 1 h. The cells were washed with PBS. The fluorescence intensity was read by the plate reader at excitation/emission of 647/668 nm, or the live images were taken by fluorescence microscopy.

GCase activity measurement

For testing the effect of PGRN knockout on GCase (β-glucocerebrosidase/*GBA*) activity, fluorescent substrate: 4-Methylumbelliferyl β-D-glucopyranoside (4-MUG) was used to determined GCase activity in cell lysate. Briefly, 20 ug cell lysate of L444P or L444P/PGRN KO fibroblasts was incubated with 4-MUG in 0.1 M citrate buffer (0.8% w/v sodium taurocholate, pH 5.2) for 1 hour at 37^{o}C. The fluorescence intensity of released 4-methylumbelliferone was measured with SpectraMax i3x plate reader (excitation wave length: 340nm; emission wavelength: 460nm), which indicated the GCase activity.

Immunofluorescence staining and confocal microscope

Frozen lung sections, cover-slip cultured L444P/PGRN KO, or PGRN KO C28i2, were fixed with 4% formaldehyde for 5 min and washed with PBS twice. The cells were permeabilized by 0.1% TritonX-100 PBS for 5 min and washed with PBS. The tissues were blocked with 1:50 dilution of normal donkey serum for 30 min. Primary antibodies were probed on the slides at 4°C over-night. The next day, slides were washed with PBS, indicated fluorescence-labeled secondary antibodies were added for 1 h and followed by wash with PBS. The tissues or cells were mounted on anti-fade medium containing DAPI. The images were taken by Leica TCS SP5 confocal system.

Construction of expression plasmids

cDNAs encoding either full-length human PGRN or its serial N-terminal or Grn E deletion mutant Δ-ND7 were cloned into pEGFP-N1 vectors by using EcoRI and BamHI sites. The amino acid number encoded by N-terminal Deletions (ND) constructs: full-length PGRN (aa 1-593), ND1 (aa 45-593), ND2 (aa 113-593), ND3 (aa 179-593), ND4 (aa 261-593), ND5 (aa 336-593), ND6 (aa 416-593), and ND7 (aa 496-593). The

amino acid number encoded by Grn E Deletion construct: Δ-ND7 (aa 1-521). All constructs were confirmed by DNA sequence.

Immunoprecipitation

Plasmids of GFP-tagged PGRN and its N-terminal deletion or Grn E deletion mutant Δ-ND7, or GFP-vector, was transfected in HEK293T cells for 48 hours. Cells were lysed by RIPA lysis and a total of 1 mg protein was used to conduct co-immunoprecipitation (Co-IP) in each sample. Anti-GFP antibody was used to perform immunoprecipitation and Rab2 antibody was used to probe the protein complex.

Co-localization analysis

To determine the colocalization of PGRN and Rab2, L444P fibroblasts were grown in glass bottom microwell dishes. When the cell confluency reached to 80%, the cells were then fixed in 4% formaldehyde for 5 min at RT. After washing steps, the cells were permeabilized with 0.1% Triton X-100 in PBS for 10 min. After further wash steps, the cells were blocked in the 1% (w/v) BSA/PBS at 4°C for 1 h. Then the cells incubated with PGRN monoclonal antibody (1:200) and Rab2 polyclonal antibody (1:200) together at 4°C overnight, followed by incubation with FITC-conjugated donkey anti-mouse IgG antibody (1:200) and Cy5-conjugated goat anti-Rabbit IgG antibody (1:200) at room temperature for 1 hour. The cells were then counterstained with 100 ng/mL 4,6-diamidino-2-phenylindole (DAPI, Molecular Probes, Cat# D1306) for 10 min. Confocal images were taken on a Zeiss LSM710-UV Confocal Microscope.

Expression and purification of ND7

The sequence for ND7 was inserted into pD444 expression vector with a His-tag (from DNA2.0, Menlo Park, CA). ND7 was expressed in the BL21(DE3) *E. coli* strain after induction by 1 mM IPTG. After a 3 h culture, cells were pelleted and sonicated to release the fusion protein. His-tagged ND7 was purified by using HIS-Select Nickel Affinity Gel (Sigma-Aldrich, Natick, MA, USA). Briefly, *E. coli* cell lysis was incubated with affinity beads overnight, and washed with washing buffer (50 mM NaH_2PO_4, 200 mM NaCl, 50 mM Imidazole, pH 8.0) six times. ND7 was eluted from beads with elution buffer (50 mM NaH_2PO_4, 200 mM NaCl, 250 mM Imidazole, pH 8.0). After dialysis with PBS, endotoxin removal using Pierce High-Capacity Endotoxin Removal Resin (Pub. Part No. 2162373.3) (Thermo Fisher Scientific (Bridgewater, NJ, USA), and 0.2 μm filter sterilization, recombinant ND7 protein was ready to be used.

Autophagic flux analysis

To determine how PGRN KO and Rab2 KO affect autophagic flux, tandem mCherry-GFP-LC3 assay was used. This assay takes advantage of the differential sensitivity to lysosomal acidity. The GFP fluorescence will be quenched in lysosomes as these are acidic compartments (pH 4 –5), whereas the fluorescence of mCherry is relatively stable and retained within lysosomes. When the protein localizes to autophagosomes, mCherry-GFP-LC3 emits both green and red fluorescence signals generating an overall yellow signal. Additionally, the fluorescence of GFP, but not of mCherry, will be quenched within

autolysosomes, making autolysosomes appear red. In this way, mCherry-GFP-LC3 tandem fluorescent-tagged LC3 can be used to visualize transition from neutral autophagosomes to acidic autolysosomes. Briefly, the indicated knockout stable cell lines (PGRN KO or Rab2 KO) were transfected with GFP-mCherry-LC3, 24 h post-transfection, the cells were treated with rapamycin at 37^{o}C overnight and the autophagic flux was analyzed by fluorescence microscopy.

Transmission electron microscope (TEM)

After OVA treatment, WT and PGRN KO mice were anesthetized and the lung was perfused with a fixative containing 2.5% glutaraldehyde and 2% paraformaldehyde in 0.1 M sodium cacodylate buffer (pH 7.2) for 2 h. After washing, the samples were postfixed in 1% OsO4 for 1 h, followed by block staining with 1% uranyl acetate for 1 h, dehydration, and finally, embedded in Embed 812 (Electron Microscopy Sciences, Hatfield, PA). 60 nm sections were cut, and stained with uranyl acetate and lead citrate by standard methods. Stained grids were examined under Philips CM-12 electron microscope (FEI; Eindhoven, Netherlands) and photographed with a Gatan (4 k × 2.7 k) digital camera (Gatan, Inc., Pleasanton, CA). The preparation of the cell samples for TEM were done with the assistance of Dr. Fengxia Liang at NYU Medical School OCS Microscopy Core.

For immunogold labeling, the mice lung tissue sections were incubated with antibody against p62, followed by incubation with secondary antibody labeled with 5 nm gold particle. Sections were observed under electron microscopy.

Statistical analysis

For comparison of treatment groups, we performed unpaired t-tests, paired t-tests, or one-way ANOVA (where appropriate). All statistical analysis was performed using GraphPad Prism 7 Software. Data are shown as mean ± SD, *$p < 0.05$, **$p < 0.01$, ***$p < 0.001$.

Results

PGRN deficiency leads to accumulation of autophagosomes in OVA-challenged PGRN null GD model

We previously reported that PGRN deficient (PGRN KO) mice developed a typical GD cellular phenotype following ovalbumin (OVA) challenge, as evidenced by enlarged macrophages reminiscent of classic Gaucher-like cells and tubular lysosomes [14]. Leveraging this GD animal model **(Fig. 1A)**, we first examined the levels of autophagy-associated molecules. One of the typical autophagosome marker is LC3, a microtubule-associated protein existing as two isoforms: LC3-I and LC3-II. A post-translational modification converts LC3-I into LC3-II, which is specifically associated with autophagosome membranes and is widely used as an autophagic marker [35, 36]. The level of LC3-II in PGRN KO OVA mice was significantly higher than that in WT OVA mice, suggesting the accumulation of autophagosomes in PGRN KO OVA mice (**Fig. 1B, C**).

Autophagy-related proteins 5 and 12 (ATG5 and ATG12) are two proteins that form a 50 kDa complex which are also involved in the formation of the autophagosome. Therefore, this dimer can be used as a detector of the presence of autophagosomes in an advanced stage of maturation of autophagosome and its accumulation is directly proportional to the accumulation of non-degraded autophagosomes [37, 38]. As shown in **Fig. 1B** and **D**, the two proteins can be observed as a complex (50 kDa) and are accumulated in tissues in PGRN KO OVA mice as compared to WT OVA mice. In addition, immunofluorescence staining of lung tissues from WT and PGRN KO mice challenged with OVA revealed much higher levels of LC3-II and ATG5 in PGRN KO OVA lung than in that in WT control as well (**Fig. 1F**, **G**).

During autophagy, damaged or misfolded proteins are ubiquitinated, and then colocalized with p62-SQSTM1 and delivered to the proteasome for degradation [39]. p62 binds to LC3-II and acts as a bridge between the substrate and the inner membrane of the autophagosome [40, 41]. p62 level is directly proportional to blockade of the autophagic flux since p62 is degraded with the cargo when the autophagic flux is completed, and its accumulation indicates the absence of autophagosome degradation [42]. We found that the expression level of p62 was markedly higher in tissues of PGRN KO OVA mice as compared to WT OVA mice **(Fig. 1B, E)**. Electron microscopy (EM) images of p62 immunogold labeling in Gaucher cells derived from murine model lung tissues exihibited significant accumulation of p62 in PGRN KO OVA mice as well, indicative of defective autophagic flux in PGRN KO OVA mice relative to WT counterparts (**Fig. 1H, I**).

Progranulin deficiency aggravates the GD phenotype in GD patient fibroblasts

Coordination between the autophagic and lysosomal degradation pathways is critical for the cellular turnover of the proteins and organelles [2]. Accordingly, we next examined the effect of PGRN deficiency upon lysosomal storage in GD patient fibroblasts. PGRN was ablated in GD type 2 patient fibroblasts (L444P) using CRISPR-Cas9 technology (**Fig. 2A**) and the knockout efficiency was confirmed by western blotting (**Fig. 2B**). As shown in **Fig. 2C** and **D**, fluorescence signal intensity, indicative of lysosomal storage content, was significantly higher in L444P/PGRN KO relative to L444P control cells, especially following lipid stimulation. We previously reported that PGRN binds directly to GCase, functioning as an indispensable adaptor for the formation of a complex between Hsp70 and GCase/LIMP2, which contributes to appropriate lysosomal localization of defective GCase in GD [14]. Consistent with our previous report [14], GCase activity was dramatically decreased in L444P/PGRN KO, as measured by fluorescence intensity of released 4-methylumbelliferone (**Fig. 2E**). In addtion, β-glucosylceramide (β-GlcCer), the substrate of GCase, was further accumulated in L444P/PGRN KO fibroblasts (**Fig. 2F**).

PGRN deficiency causes autophagosome accumulation in GD patient fibroblasts

Given that autophagosome markers, such as LC3-II, ATG5-ATG12 complex and p62, accumulate in PGRN KO mice with OVA challenge (**Fig. 1**), we next employed western blotting to measure these molecular markers of autophagy in L444P GD patient fibroblasts in the presence or absence of PGRN. As shown in **Fig. 3A-D**, the LC3-II and ATG5-ATG12 complex levels were significantly increased in L444P/PGRN KO in comparison with L444P cells. Elevated LC3-II level could result from early stage initiation of autophagy or

by blockade of autophagic flux at late stage. Notably, p62, one of the molecular markers of autophagic flux, was also significantly increased in L444P/PGRN KO relative to control L444P fibroblasts, which strongly suggested accumulation of autophagic substrates. Moreover, immunofluorescence staining supported western blotting results (**Fig. 3E-H**). In summary, the increased levels of LC3-II and p62 indicated that late stage of autophagy was defective in PGRN deficient L444P patient fibroblasts.

PGRN deficiency impairs autophagosome-lysosome fusion

The neoformed autophagosome goes through two stages of maturation before fusion, and EM could be employed to distinguish the double-membrane of an immature autophagosome from the single-membrane of the lysosome-fused late autophagosome [43]. EM images acquired from WT OVA murine macrophages highlighted the predominance of singe-membraned autophagic vacuoles, while macrophages isolated from PGRN KO OVA mice highlighted predominance of double-membraned initial autophagic vacuoles (**Fig. 4A**). These data demonstrated that the deficiency of PGRN resulted in defects in late stage autophagy. Accorrdingly, visualization of L444P and L444P/PGRN KO cells using EM revealed a greater abundance of autophagosome initial vacuole in L444P/PGRN KO compared with L444P (**Fig. 4B, C**).

To further confirm the association between PGRN deficiency and a defect of autophagosome-lysosome fusion, the subcellular localizations of the autophagic marker LC3 and the lysosomal protein LIMP2 were investigated with confocal microscopy in L444P/PGRN KO fibroblasts [44]. As shown in **Fig. 4D** and **E**, co-localization of LC3 and LIMP2 was significantly reduced in L444P/PGRN KO compared with L444P fibroblasts. PGRN KO C28I2 chondrocytes **(Supplementary Fig. 1A**) were also used to examine the co-localization of LC3 and LIMP2. Similarly, co-localization of LIMP2 and LC3 was significantly reduced in PGRN KO C28I2 cells as compared to control cells under rapamycin stimulation (**Supplementary Fig. 1D**). In addition, the LC3 accumulation was also observed in PGRN KO C28I2 cells (**Supplementary Fig. 1B, C**). These data suggested that PGRN regulation of autophagosome-lysosome fusion in autophagy may be a mechanism common across different cell types.

In addtion, we tested the autophagic flux, which represented autophagosome-autolysosome formation and degradation, in GD fibroblasts using mCherry-GFP-LC3 assay. Compartment specific differential quenching of GFP and mRFP fluorescence signals allows the use of mCherry-GFP-LC3 for assessment of the number of autophagosomes and autolysosomes, and quantification of autophagic flux [42, 45, 46]. As shown in **Fig. 4F** and **G**, green puncta, which represented the unfused autophagosome, were significantly increased in L444P/PGRN KO compared with L444P, especially after rapamycin stimulation. The numbers of red and green punta were quantified with normalization to cell count and the difference between red puncta and green puncta was taken as representative of the autophagic flux. From **Fig. 4G**, we can see the autophagic flux was increased after rapamycin stimulation in L444P, however, no clear change was observed in L444P/PGRN KO with or without rapamycin stimulation, which suggested that autophagosome-autolysosome formation was defect in PGRN deficiency L444P (**Fig. 4F, G**).

Progranulin binds to Rab2 and Grn E of PGRN is the major domain responsible for Rab2 interaction

After the maturation of the autophagosome, the autophagosome and lysosome move closer together and fuse. Once fusion is complete, the contents of the autophagosome are exposed to the lysosome and are degraded by the lysosomal hydrolases [47, 48]. Various tethering factors contribute to autophagosome-lysosome fusion. SNAREs are reported to be the core machinery for fusion, the autophagosomal Q-soluble N-ethylmaleimide-sensitive factor attachment protein receptor (SNARE) protein syntaxin 7 (STX17) interacts with endosomal/lysosomal R-SNARE VAMP8 to form a trans-SNARE complex, which mediates autophagosome-lysosome fusion [49]. Consecutive RAB-mediation is a critical tethering step for autophagosome-lysosome fusion. RABs are small GTPases, which regulate autophagic membrane traffic [50, 51]. Rab7 is most widely assumed to regulate autophagosome-lysosome fusion by interacting with various tethering factors [52, 53]. However, a growing body of reports suggest that Rab2 is another critical GTPase mediator of autophagy [54-56]. In our present study, PGRN deficient cells presented with impaired autophagosome-lysosome fusion. We thus hypothesized that PGRN may associate with these aforementioned critical tethering factors including VAMP8, Rab7, or Rab2. To test this hypothesis, we used Nickel beads to pull down His-tagged PGRN and then the precipitated His-tagged PGRN complex was immunoblotted onto a nitrocellulose membrane followed by detection with antibodies against VAMP8, Rab7, or Rab2. As shown in **Fig. 5A**, Rab2 was co-purified with PGRN, indicating the physical interaction between PGRN and Rab2. However, VAMP8 or Rab7 was not detectable in precipitated PGRN complex solution. In addition, co-immunoprecipitation (Co-IP) further demonstrated the interaction between endogenous PGRN and Rab2 in L444P patient fibroblasts (**Fig. 5B**).

To identify the domains of PGRN required for interacting with Rab2, serial GFP-tagged N-terminal deletions of PGRN were constructed (**Fig. 5C**). Co-IP was performed using the same amounts of these mutants to examine their bindings to endogenous Rab2. As shown in **Fig. 5D**, the binding of PGRN with Rab2 became more pronounced following deletion of Grn P (ND1); binding became weaker with further deletion of Grn F (ND3) and most weak following deletion of Grn B (ND2 and ND3, respectively). These results suggest that Grn P and B might act as regulatory domains for the binding to Rab2. The Grn E (ND7) fragment exhibited strong binding ability undistinguisbable to that of full-length PGRN. Interestingly, our previous study found that the Grn E domain was also required and sufficient for PGRN binding to GCase [14]. To further determine whether this Grn E domain is similarly critical for binding with Rab2, a PGRN mutant with E domain deletion (Δ-ND7) was constructed; Co-IP revealed markedly reduced binding between Δ-ND7 and Rab2 relative to the interaction observed between full-length PGRN and Rab2 (**Fig. 5D**). Collectively, PGRN has morn than one domain involved in the interactions with Rab2, but the C-terminal fragment of PGRN (amino acids 496-593), named ND7, is both required and sufficient for the full interaction with Rab2. In addtion, the association of PGRN and Rab2 was further confirmed by their colocalization in L444P fibroblats **(Fig. 5E),** which supported the interaction between PGRN and Rab2.

Rab2 deficiency accumulated autophagic markers and defected autophagic flux in L444P GD fibroblasts

Each stage of dynamic autophagic processing, including autophagosome formation, autolysosome formation and lysosomal degradation intracellular membrane dynamics, is regulated by members of the Ras-like GTPase superfamily - primarily comprised of Rab proteins [50]. Several specific autophagic roles

of individual Rab GTPases have been identified and Rab2 has been recognized as a crucial regulator in formation of autophagosome and autolysosome [54, 57]. To clarify whether binding between Rab2 and PGRN contributes to the role of Rab2 in autophagosome-autolysosome formation in GD, we also established a stable Rab2 KO L444P fibroblasts (L444P/Rab2 KO) using CRISPR-Cas9 technology (**Supplementary Fig. 2A**). Expression levels of autophagic makers LC3 and p62 were analysed in L444P or L444P/Rab2 KO. As shown in **Supplementary Fig. 2B-D**, the levels of both LC3-II and p62 were increased in Rab2 KO deficiency L444P, which indicated that the Rab2 deficiency leads to the defect of the late stage of autophagy in L444P. Autophagic flux was also measured using tandem mCherry-GFP-LC3 assay. As shown in **supplementary Fig. 2E** and **F**, the red puncta, which represent LC3 activation, were increased in both L444P and L444P/Rab2 KO under rapamycin stimulation. These data suggested that the activation of autophagy was not affected by the loss of Rab2. However, the green puncta, which represent unfused autophagosomes, were much more abundant in L444P/Rab2 KO compared with control L444P with or without rapamycin stimulation. Quantification of red puncta and green puncta, illustrative of the autophagic flux, revealed significantly lower flux in L444P/Rab2 KO than in control L444P under rapamycin stimulation (**Supplementary Fig. 2E, F**). These data revealed that autophagosome-autolysosome formation was blocked in L444P/Rab2 KO GD patient fibroblasts, consistent with previous reports using U2OS and HEK293 cell lines [54].

As Rab2 was identified as a binding partner of PGRN, we performed WB and RT-PCR to examine the potential effect of Rab2 deficiency on the protein and mRNA levels of PGRN. Interestingly, the protein level of PGRN was decreased in L444P/Rab2 KO (**Supplementary Fig. 2G**), however, the mRNA level of PGRN was not affected by Rab2 deficiency (**Supplementary Fig. 2H**), which suggested that Rab2 may also regulate PGRN at post-transcriptional levels, such as translation and stability of PGRN, in addition to physical interactions to each other.

PGRN derived ND7 effectively ameliorates autophagy defects in GD patient fibroblasts

In our previous study, we found that Grn E is a critical domain for the binding of PGRN to GCase [14]. Interestingly, Grn E domain is also required for PGRN-Rab2 interaction (**Fig. 5**). Accordingly, we expressed and purified this C-terminal 98 amino acid fragment of PGRN containing Grn E, termed ND7 (**Fig. 6A, B**), and tested whether it is sufficient for the mediation of autophagosome-lysosome fusion. First, L444P or L444P/PGRN KO fibroblasts were transfected with GFP-fused vector, or GFP-fused full-length PGRN, or GFP-fused ND7. 24 h later, the transfected cells were stimulated with rapamycin for another 24 h. Western blotting reveals reduced levels of LC3-II and p62 in full-length PGRN or ND7 transfected L444P/PGRN KO fibroblasts relative to GFP vector transfected L444P/PGRN KO; moreover, the LC3-II and p62 expression were comparable between full-length PGRN or ND7 tranfected L444P/PGRN KO fibroblasts and the control L444P (**Fig. 6C**).

We next tested the effect of ND7 on the formation of autophagosome using EM. From **Fig. 6D, E,** we observed that L444P/PGRN KO fibroblasts treated with ND7 exhibited a shift toward prevalence of advanced degradative vacuoles to a degree comparable with L444P. mCherry-GFP-LC3 assay revealed

that green puncta, which represent the unfused autophagosome, were significantly decreased in ND7 treated L444P/PGRN KO compared with untreated L444P/PGRN KO under rapamycin stimulation (**Fig. 6F, G**). Moreover, autophagic flux was also increased in ND7 treated L444P/PGRN KO (**Fig. 6F, G**). Taken together, ND7 administration could rescue the autophagic defect in PGRN KO GD L444P fibroblasts. Morever, in lung tissues of OVA-challenged PGRN KO mice, levels of LC3-II and p62 also decreased drastically after ND7 administration as assessed by western blotting (**Supplementary Fig. 3A**). In line with these results, immunofluorescence staining for LC3 also revealed that ND7 could significantly decrease the levels of LC3-II and P62 (**Supplementary Fig. 3B**).

Discussion

Our previous studies demonstrated that PGRN KO mice presented with Gaucher cells in lung tissues, especially after OVA challenge, and this GD cellular phenotype could be ameliorated by administration of recombinant PGRN and its derivative, indicating a critical role of PGRN in GD pathogenesis and theraputic intervention [14, 32]. It was also reported that PGRN deficiency associates with reduced autophagic flux in neurons and impaired autophagy in neuropathic diseases [28]. Moreover, screening for regulatory genes targeting neuronal PGRN expression has revealed enrichment of genes from the autophagy–lysosome pathway; in turn, modulating PGRN expression exerts regulatory effects upon the autophagy-lysosome pathway [34, 58]. In current study, we observed elevated expressions of LC3-II, p62 and ATG5-ATG12 complex in PGRN KO tissues, especially after OVA challenge, indicating accumulation of autophagosomes in PGRN deficient mice (**Fig. 1B-E**). Notably, PGRN is capable of activating the upstream modulators of mechanistic target of rapamycin and, in turn, mTOR signaling [30, 59]. mTOR signaling contributes to the regulation of various fundamental cell processes including autophagy, with stimulation of mTORC1, but not mTORC2, inhibitive of autophagy [34, 58, 60-62]. Accordingly, increased levels of LC3-II and ATG5/ATG12 complex in PGRN KO mice, particularly under stress associated with OVA challenge, may be resultant of reduced activation of the mTOR signaling pathway associated with PGRN deficiency. Interestingly, accumulated p62 was also observed in the tubular-like lysosomes of macrophages from PGRN KO mice after OVA challenge (**Fig. 1H, I**). Accumulated p62 suggests the absence of autophagosome degradation in PGRN deficient mice, which could be due to the inhibtion of initial stage of autophgy or the defect in autophagosome-lysosome fusion [3]. The increased levels of LC3-II and ATG5/ATG12 complex, markers for autophagy initial stage, indicated that the autophagosome-lysosome fusion, but not autophagy initiation, was defective in PGRN deficient cells/mice, which, in turn, led to impaired clearance of autophagosome proteins in PGRN KO mice.

To complement our *in vivo* murine data, PGRN was also knocked out in neuropathic GD type 2 L444P patient fibroblasts using CRISPR-Cas9 (**Fig. 2A, B**). Based on the known therapeutic effects of PGRN in GD animal models [14], it is no surprising to detect higher lysosome storage content in L444P/PGRN KO patient fibroblasts (**Fig. 2C, D**). The loss of PGRN's facilitory role in posttranslational modification of GCase is expected to contribute to the decreased GCase activity and its accumulated substrate β-glucosylceramide (β-GlcCer) in L444P/PGRN KO (**Fig. 2E, F**). Consistent with *in vivo* results, the levels of LC3-II, p62 and ATG5/ATG12 complex were all increased in L444P/PGRN KO compared with the L444P

cells (**Fig. 3**). Increased LC3-II level and p62 levels observed in control group suggested the defective lysosome degradtion in GD patient L444P fibroblats. Although increased LC3-II level could be induced by either activated autophagy or inhibited autophagosome degradation [3], the observation of increased p62 levels without rapamycin stimulation bolsters the conclusion that autophagosome degradation is blocked in L444P/PGRN KO fibroblasts, which may slow the decay of LC3-II. Acting as a co-chaperone of GCase and HSP70 complex, PGRN is known to play an important role in GCase lysosomal localization [14]. PGRN deficiency in L444P may worsen the defective lysosome degradtion in patient fibroblasts. Rapamycin stimulation, which induces autophagy through inhibition of mTOR activity, had no effect on the levels of LC3-II and p62 in L444P/PGRN KO fibroblasts. In L444P/PGRN KO, inhibition of the mTOR signaling pathway caused by PGRN deficiency may occlude observation of the effects of the rapamycin.

Autophagosome-autolysosome fusion is an obligatory step for the clearance of the autophagosomes in late-stage of autophagy [63]. We also evaluated fusion in the presence and absence of PGRN by visualization of differential morphology of autophagosomes and autolysosomes under EM [64]. In the GD-like macrophages from PGRN KO mice, most of the autophagic vacuoles exhibit the double membrane characteristic of autophagosomes [65]; while in WT mice, most of the autophagic vacuoles were identifiable as single membraned autolysosomes, indicating that PGRN deficiency leads to a defect in fusion between autophagosome and lysosome. Defective autophagosome-lysosome fusion was further confirmed by the decreased co-localization of autophagosome marker LC3 and lysosome marker LIMP2 in PGRN deficient cells, both in L444P GD fibroblasts and C28I2 cells (**Figs. 4, 6, Supplementary Fig. 1D**). These results are in agreement with a previous report concerning PGRN deficiency mediated impairment of autophagic flux driven by an diminished clearance of autophagosomes [28].

In an effort to investigate the mechanism underlying impaired autophagosome and lysosome fusion in PGRN KO cells, we examined whether PGRN associates with several reported critical tethering factors: VAMP8, Rab7 and Rab2. Intriguingly, we found that PGRN selectively interacts with Rab2, and the Grn E domain is critical for this interaction (**Fig. 5D**). Recent studies have demonstrated that Rab2 plays an important role in autophagy through acting as a key factor for autophagic and endocytic cargo delivery and degradation in lysosomes [55, 56] and as a regulator of the formation of autophagosome and autolysosome in mammalian cells [54]. Consistantly the deficiency of Rab2 aggravated the defective autophgy degradtion in L444P patient fibroblats. Furhtermore, autophagic flux was impaired alongside downregulation of PGRN protein expression in Rab2 KO L444P fibroblasts (**Supplementary Fig. 2**). Taken together, the findings in this study demonstrate that PGRN physically interacts with Rab2 and both proteins are needed to link autophagosomes and lysosomes together, i.e. fuse; and deficiency of either PGRN or Rab2 impairs autophagosome-lysosome fusion, which in turn leading to the accumulation of autophagosomes.

Mitochondria produce reactive oxygen species (ROS) in response to changes in the intracellular environment. Increased ROS production in turn causes mitochondrial defects and the oxidative damage produced by free radicals is extensive in the lungs of mice treated with OVA [65]. Accumulation of damaged mitochondria is toxic and the cell has developed a type of specific autophagy, called

mitophagy, as a defense mechanism to promote removal of these organelles [66, 67]. Accordingly, we also monitored mitochondrial morphology and markers of mitophagy in GD macrophages of WT and PGRN KO mice after OVA challenge. OVA-challenged PGRN KO mice exhibited consistent mitochondrial damage (**Supplementary Fig. 4A**). Bcl2-L13 is the mammalian homolog of mitophagy-specific gene *Atg32*, the protein product of which recognizes damaged mitochondria and accompanies them to degradation [68, 69]. Consistent with EM images, immunofluorescence imaging of Bcl2-L13 from PGRN KO OVA mice tissues illustrated significant accumulation of Bcl2-L13 relative to levels observed in tissues extracted from WT OVA mice (**Supplementary Fig. 4B)**. In addition, PGRN or ND7 administration restored Bcl2-L13 expression level, indicating that treatment favors the clearance of damaged mitochondria (**Supplementary Fig. 4C**). Prior work has noted defective mitochondrial function and mitophagy in association with *GBA* mutations [10, 11, 70, 71]. In our GD model, OVA-challenged PGRN KO developed a GD phenotype in a manner independent of *GBA* mutation; therefore, a disparate mechanism may underlie the accumulation of damaged mitochondria in OVA-challenged PGRN KO mice. While accumulation of damaged mitochondria in PGRN KO mice after OVA challenge may be caused by impaired autophagosome-lysosome fusion, the effect of PGRN on mitophagy in GD warrants further investigation.

PGRN, particularly its derivative ND7, may be a new treatment for patients with GD. However, Additional investigations with additional GD models are needed to further test its therapeutic effect and safety. Moreover, it would be interesting to further investigate the role of PGRN in additional stages of autophagy in GD and other lysosomal storage diseases. Given the importance of autophagy in Gaucher Disease, the therapeutic potential of autophagy is of great importance. The identification of PGRN deficiency/insufficiency as a risk factor for GD is certainly a source of considerable excitement in the field, especially after the confirmation of its involvement in autophagy in GD. This study is the first to identify PGRN as a novel factor required for autophagosome-lysosome fusion, thus providing a solid foundation for future discoveries relating to this critical factor in autophagy and probably mitophagy as well. More importantly, this study yields the discovery of an approximately 15-kDa PGRN derivative (i.e. ND7) that effectively ameliorates PGRN deficiency caused defects in autophagy as well as GD phenotypes. In brief, this study carries the potential, not only for future advances in understanding autophagy in relation to the pathogenesis of GD, but also for the development of novel therapies to combat GD, particularly neuronopathic GD which currently lacks the drugs/treatments.

Abbreviations

ATG5: autophagy related 5; ATG12: autophagy related 12; ATG16L1: autophagy related 16 like 1; Ctrl: control; EM: Electron microscopy; GCase: β-glucocerebrosidase; GD: Gaucher disease; GFP: green fluorescent protein; Grn: Granulin; HSP70: 70 kilodalton heat shock proteins; IP: immunoprecipitation; KO: knockout; LC3: microtubule-associated protein 1 light chain 3; LIMP2: Lysosomal integral membrane protein 2; LSD: lysosome storage disease; β-GlcCer: β-glucosylceramide; ND: N-terminal deletion; OVA: ovalbumin; PGRN: progranulin; Rab2: Ras-related protein Rab-2A; Rab7: Ras-related protein Rab-7a; RUBCNL/PACER: rubicon like autophagy enhancer; SQSTM1/p62: sequestosome 1; STX17: syntaxin 17;

TNF: Tumor Necrosis Factor; VAMP8: Vesicle-associated membrane protein 8; WB: western blot; WT: wild type.

Declarations

Ethics approval The full name of the Ethic Committee, from which a written approval was obtained allowing to carry out the experiments, is stated in the “Materials and methods” section.

Consent to participate Not applicable

Consent for publication Not applicable

Data transparency All authors confirm that all data and material support their published claims and comply with field standards.

Conflict of interest The authors declare no competing interests.

Acknowledgments

We thank Drs. Yan Deng and Fengxia Liang at NYU Medical School OCS Microscopy Core for their assistance with confocal and electronic microscope image. We also thank all lab members for the insightful discussions. All authors disclose no conflict of interest. Patents have been filed by NYU that claim PGRN and its derivatives for diagnosis and treatment of Gaucher disease (PCT/US2015014364).

Author Contributions

X. Zhao, J. Jian, R. Liberti and W. Fu designed and performed experiments, collected and analyzed data, and wrote the paper. A. Hettinghouse assisted with experiments and editing the manuscript. C. J. Liu supervised this study, analyzed data, and co-wrote and edited the manuscript.

Funding

This work was supported partly by NIH research grants R01NS103931, R01AR062207, R01AR061484 and R01AR076900 (CJ Liu).

References

1. Glick, D., S. Barth, and K.F. Macleod, *Autophagy: cellular and molecular mechanisms.* J Pathol, 2010. **221**(1): p. 3-12.
2. Settembre, C., et al., *Lysosomal storage diseases as disorders of autophagy.* Autophagy, 2008. **4**(1): p. 113-4.
3. Kinghorn, K.J., A.M. Asghari, and J.I. Castillo-Quan, *The emerging role of autophagic-lysosomal dysfunction in Gaucher disease and Parkinson's disease.* Neural Regen Res, 2017. **12**(3): p. 380-384.

4. Seranova, E., et al., *Dysregulation of autophagy as a common mechanism in lysosomal storage diseases.* Essays Biochem, 2017. **61**(6): p. 733-749.
5. Platt, F.M., *Sphingolipid lysosomal storage disorders.* Nature, 2014. **510**(7503): p. 68-75.
6. Chen, Y., et al., *Molecular regulations and therapeutic targets of Gaucher disease.* Cytokine Growth Factor Rev, 2018. **41**: p. 65-74.
7. Grabowski, G.A., *Gaucher disease and other storage disorders.* Hematology Am Soc Hematol Educ Program, 2012. **2012**: p. 13-8.
8. Pitcairn, C., W.Y. Wani, and J.R. Mazzulli, *Dysregulation of the autophagic-lysosomal pathway in Gaucher and Parkinson's disease.* Neurobiol Dis, 2019. **122**: p. 72-82.
9. Sun, Y. and G.A. Grabowski, *Impaired autophagosomes and lysosomes in neuronopathic Gaucher disease.* Autophagy, 2010. **6**(5): p. 648-9.
10. Li, H., et al., *Mitochondrial dysfunction and mitophagy defect triggered by heterozygous GBA mutations.* Autophagy, 2019. **15**(1): p. 113-130.
11. Moren, C., et al., *GBA mutation promotes early mitochondrial dysfunction in 3D neurosphere models.* Aging (Albany NY), 2019. **11**(22): p. 10338-10355.
12. Li, S.S., et al., *Reduction of PGRN increased fibrosis during skin wound healing in mice.* Histol Histopathol, 2019. **34**(7): p. 765-774.
13. Jian, J., J. Konopka, and C. Liu, *Insights into the role of progranulin in immunity, infection, and inflammation.* J Leukoc Biol, 2013. **93**(2): p. 199-208.
14. Jian, J., et al., *Progranulin Recruits HSP70 to beta-Glucocerebrosidase and Is Therapeutic Against Gaucher Disease.* EBioMedicine, 2016. **13**: p. 212-224.
15. Jian, J., et al., *Progranulin: A key player in autoimmune diseases.* Cytokine, 2018. **101**: p. 48-55.
16. Bateman, A. and H.P. Bennett, *The granulin gene family: from cancer to dementia.* Bioessays, 2009. **31**(11): p. 1245-54.
17. Cui, Y., A. Hettinghouse, and C.J. Liu, *Progranulin: A conductor of receptors orchestra, a chaperone of lysosomal enzymes and a therapeutic target for multiple diseases.* Cytokine Growth Factor Rev, 2019. **45**: p. 53-64.
18. Bateman, A., S.T. Cheung, and H.P.J. Bennett, *A Brief Overview of Progranulin in Health and Disease.* Methods Mol Biol, 2018. **1806**: p. 3-15.
19. Baker, M., et al., *Mutations in progranulin cause tau-negative frontotemporal dementia linked to chromosome 17.* Nature, 2006. **442**(7105): p. 916-9.
20. Arrant, A.E., et al., *Restoring neuronal progranulin reverses deficits in a mouse model of frontotemporal dementia.* Brain, 2017. **140**(5): p. 1447-1465.
21. Gotzl, J.K., et al., *Common pathobiochemical hallmarks of progranulin-associated frontotemporal lobar degeneration and neuronal ceroid lipofuscinosis.* Acta Neuropathol, 2014. **127**(6): p. 845-60.
22. Mendsaikhan, A., I. Tooyama, and D.G. Walker, *Microglial Progranulin: Involvement in Alzheimer's Disease and Neurodegenerative Diseases.* Cells, 2019. **8**(3).

23. Chitramuthu, B.P., H.P.J. Bennett, and A. Bateman, *Progranulin: a new avenue towards the understanding and treatment of neurodegenerative disease.* Brain, 2017. **140**(12): p. 3081-3104.
24. Tang, W., et al., *The growth factor progranulin binds to TNF receptors and is therapeutic against inflammatory arthritis in mice.* Science, 2011. **332**(6028): p. 478-84.
25. Jian, J., et al., *Progranulin directly binds to the CRD2 and CRD3 of TNFR extracellular domains.* FEBS Lett, 2013. **587**(21): p. 3428-36.
26. Liu, C., et al., *Progranulin-derived Atsttrin directly binds to TNFRSF25 (DR3) and inhibits TNF-like ligand 1A (TL1A) activity.* PLoS One, 2014. **9**(3): p. e92743.
27. Li, M., et al., *Progranulin is required for proper ER stress response and inhibits ER stress-mediated apoptosis through TNFR2.* Cell Signal, 2014. **26**(7): p. 1539-48.
28. Chang, M.C., et al., *Progranulin deficiency causes impairment of autophagy and TDP-43 accumulation.* J Exp Med, 2017. **214**(9): p. 2611-2628.
29. Guo, Q., et al., *Progranulin causes adipose insulin resistance via increased autophagy resulting from activated oxidative stress and endoplasmic reticulum stress.* Lipids Health Dis, 2017. **16**(1): p. 25.
30. Zhou, B., et al., *Progranulin induces adipose insulin resistance and autophagic imbalance via TNFR1 in mice.* J Mol Endocrinol, 2015. **55**(3): p. 231-43.
31. Liu, J., et al., *PGRN induces impaired insulin sensitivity and defective autophagy in hepatic insulin resistance.* Mol Endocrinol, 2015. **29**(4): p. 528-41.
32. Jian, J., et al., *Association Between Progranulin and Gaucher Disease.* EBioMedicine, 2016. **11**: p. 127-137.
33. Chen, Y., et al., *Progranulin associates with hexosaminidase A and ameliorates GM2 ganglioside accumulation and lysosomal storage in Tay-Sachs disease.* J Mol Med (Berl), 2018. **96**(12): p. 1359-1373.
34. Elia, L.P., et al., *Genetic Regulation of Neuronal Progranulin Reveals a Critical Role for the Autophagy-Lysosome Pathway.* J Neurosci, 2019. **39**(17): p. 3332-3344.
35. Tooze, S.A. and T. Yoshimori, *The origin of the autophagosomal membrane.* Nat Cell Biol, 2010. **12**(9): p. 831-5.
36. Parzych, K.R. and D.J. Klionsky, *An overview of autophagy: morphology, mechanism, and regulation.* Antioxid Redox Signal, 2014. **20**(3): p. 460-73.
37. Mizushima, N., *The ATG conjugation systems in autophagy.* Curr Opin Cell Biol, 2020. **63**: p. 1-10.
38. Romanov, J., et al., *Mechanism and functions of membrane binding by the Atg5-Atg12/Atg16 complex during autophagosome formation.* EMBO J, 2012. **31**(22): p. 4304-17.
39. Chen, M., et al., *TRIM14 Inhibits cGAS Degradation Mediated by Selective Autophagy Receptor p62 to Promote Innate Immune Responses.* Mol Cell, 2016. **64**(1): p. 105-119.
40. Lamark, T., S. Svenning, and T. Johansen, *Regulation of selective autophagy: the p62/SQSTM1 paradigm.* Essays Biochem, 2017. **61**(6): p. 609-624.

41. Danieli, A. and S. Martens, *p62-mediated phase separation at the intersection of the ubiquitin-proteasome system and autophagy.* J Cell Sci, 2018. **131**(19).
42. Yoshii, S.R. and N. Mizushima, *Monitoring and Measuring Autophagy.* Int J Mol Sci, 2017. **18**(9).
43. Eskelinen, E.L., *Maturation of autophagic vacuoles in Mammalian cells.* Autophagy, 2005. **1**(1): p. 1-10.
44. Settembre, C., et al., *A block of autophagy in lysosomal storage disorders.* Hum Mol Genet, 2008. **17**(1): p. 119-29.
45. Matus, S., V. Valenzuela, and C. Hetz, *A new method to measure autophagy flux in the nervous system.* Autophagy, 2014. **10**(4): p. 710-4.
46. von Muhlinen, N., *Methods to Measure Autophagy in Cancer Metabolism.* Methods Mol Biol, 2019. **1928**: p. 149-173.
47. Yu, L., Y. Chen, and S.A. Tooze, *Autophagy pathway: Cellular and molecular mechanisms.* Autophagy, 2018. **14**(2): p. 207-215.
48. Chen, Y. and L. Yu, *Development of Research into Autophagic Lysosome Reformation.* Mol Cells, 2018. **41**(1): p. 45-49.
49. Itakura, E., C. Kishi-Itakura, and N. Mizushima, *The hairpin-type tail-anchored SNARE syntaxin 17 targets to autophagosomes for fusion with endosomes/lysosomes.* Cell, 2012. **151**(6): p. 1256-69.
50. Takats, S., et al., *Small GTPases controlling autophagy-related membrane traffic in yeast and metazoans.* Small GTPases, 2018. **9**(6): p. 465-471.
51. Nakamura, S. and T. Yoshimori, *New insights into autophagosome-lysosome fusion.* J Cell Sci, 2017. **130**(7): p. 1209-1216.
52. Kuchitsu, Y. and M. Fukuda, *Revisiting Rab7 Functions in Mammalian Autophagy: Rab7 Knockout Studies.* Cells, 2018. **7**(11).
53. Jager, S., et al., *Role for Rab7 in maturation of late autophagic vacuoles.* J Cell Sci, 2004. **117**(Pt 20): p. 4837-48.
54. Ding, X., et al., *RAB2 regulates the formation of autophagosome and autolysosome in mammalian cells.* Autophagy, 2019. **15**(10): p. 1774-1786.
55. Lorincz, P., et al., *Rab2 promotes autophagic and endocytic lysosomal degradation.* J Cell Biol, 2017. **216**(7): p. 1937-1947.
56. Lund, V.K., K.L. Madsen, and O. Kjaerulff, *Drosophila Rab2 controls endosome-lysosome fusion and LAMP delivery to late endosomes.* Autophagy, 2018. **14**(9): p. 1520-1542.
57. Fujita, N., et al., *Genetic screen in Drosophila muscle identifies autophagy-mediated T-tubule remodeling and a Rab2 role in autophagy.* Elife, 2017. **6**.
58. Altmann, C., et al., *Progranulin overexpression in sensory neurons attenuates neuropathic pain in mice: Role of autophagy.* Neurobiol Dis, 2016. **96**: p. 294-311.
59. Feng, T., et al., *Growth factor progranulin promotes tumorigenesis of cervical cancer via PI3K/Akt/mTOR signaling pathway.* Oncotarget, 2016. **7**(36): p. 58381-58395.

60. Saxton, R.A. and D.M. Sabatini, *mTOR Signaling in Growth, Metabolism, and Disease.* Cell, 2017. **168**(6): p. 960-976.
61. Codogno, P. and A.J. Meijer, *Autophagy and signaling: their role in cell survival and cell death.* Cell Death Differ, 2005. **12 Suppl 2**: p. 1509-18.
62. Noda, T., *Regulation of Autophagy through TORC1 and mTORC1.* Biomolecules, 2017. **7**(3).
63. Lorincz, P. and G. Juhasz, *Autophagosome-Lysosome Fusion.* J Mol Biol, 2019.
64. Eskelinen, E.L., *To be or not to be? Examples of incorrect identification of autophagic compartments in conventional transmission electron microscopy of mammalian cells.* Autophagy, 2008. **4**(2): p. 257-60.
65. Reddy, P.H., *Mitochondrial Dysfunction and Oxidative Stress in Asthma: Implications for Mitochondria-Targeted Antioxidant Therapeutics.* Pharmaceuticals (Basel), 2011. **4**(3): p. 429-456.
66. Sachdeva, K., et al., *Environmental Exposures and Asthma Development: Autophagy, Mitophagy, and Cellular Senescence.* Front Immunol, 2019. **10**: p. 2787.
67. Garza-Lombo, C., et al., *Redox homeostasis, oxidative stress and mitophagy.* Mitochondrion, 2020. **51**: p. 105-117.
68. Kanki, T., et al., *Atg32 is a mitochondrial protein that confers selectivity during mitophagy.* Dev Cell, 2009. **17**(1): p. 98-109.
69. Kinya Otsu., e.a., *BCL2L13 is a mammalian homolog of the yeast mitophagy receptor Atg32.* Autophgy, 2015: p. 1932–1933.
70. Gegg, M.E. and A.H. Schapira, *Mitochondrial dysfunction associated with glucocerebrosidase deficiency.* Neurobiol Dis, 2016. **90**: p. 43-50.
71. Osellame, L.D. and M.R. Duchen, *Defective quality control mechanisms and accumulation of damaged mitochondria link Gaucher and Parkinson diseases.* Autophagy, 2013. **9**(10): p. 1633-5.

Figures

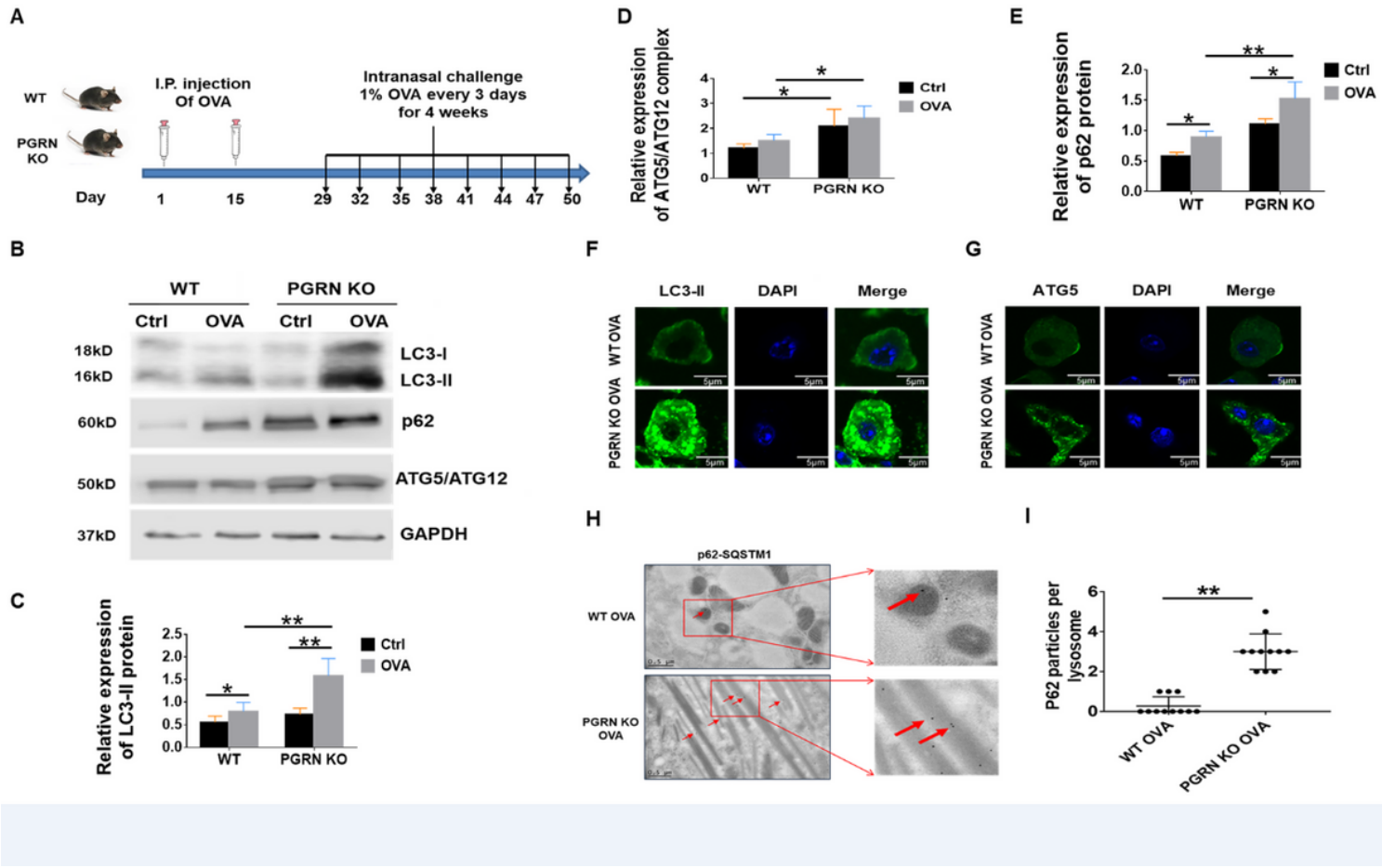

Figure 1

OVA-challenged PGRN KO mice exhibit autophagosome accumulation. (A) Diagram of the protocol for establishing the mouse model of chronic lung inflammation. WT and PGRN KO mice received I.P. injection of OVA at Day 1 and 15, followed by intranasal challenge of 1% OVA beginning at Day 29 and administrated thereafter three times a week for another four weeks. (B) Western blot analysis of LC3, p62, and ATG5/ATG12 complex levels in lung tissues extracted from WT or PGRN KO mice challenged with or without OVA. (C-E) Quantification analysis of LC3-II (C), ATG5/ATG12 complex(D) and LC3 (E) expression level. (F) Immunofluorescence staining of LC3 in lung tissues from WT and PGRN KO mice after the OVA challenge. (G) Immunofluorescence staining of ATG5 in lung tissues from WT and PGRN KO mice after the OVA challenge. (H) p62-SQSTM1 (arrows) levels assayed by immunogold labeling TEM of lung tissue from WT and KO mice after the OVA challenge. (I) Quantification analysis of H. C, D, E and I, data are mean ± SD; n ≥ 5 mice per group; * p< 0.05 or ** p < 0.01.

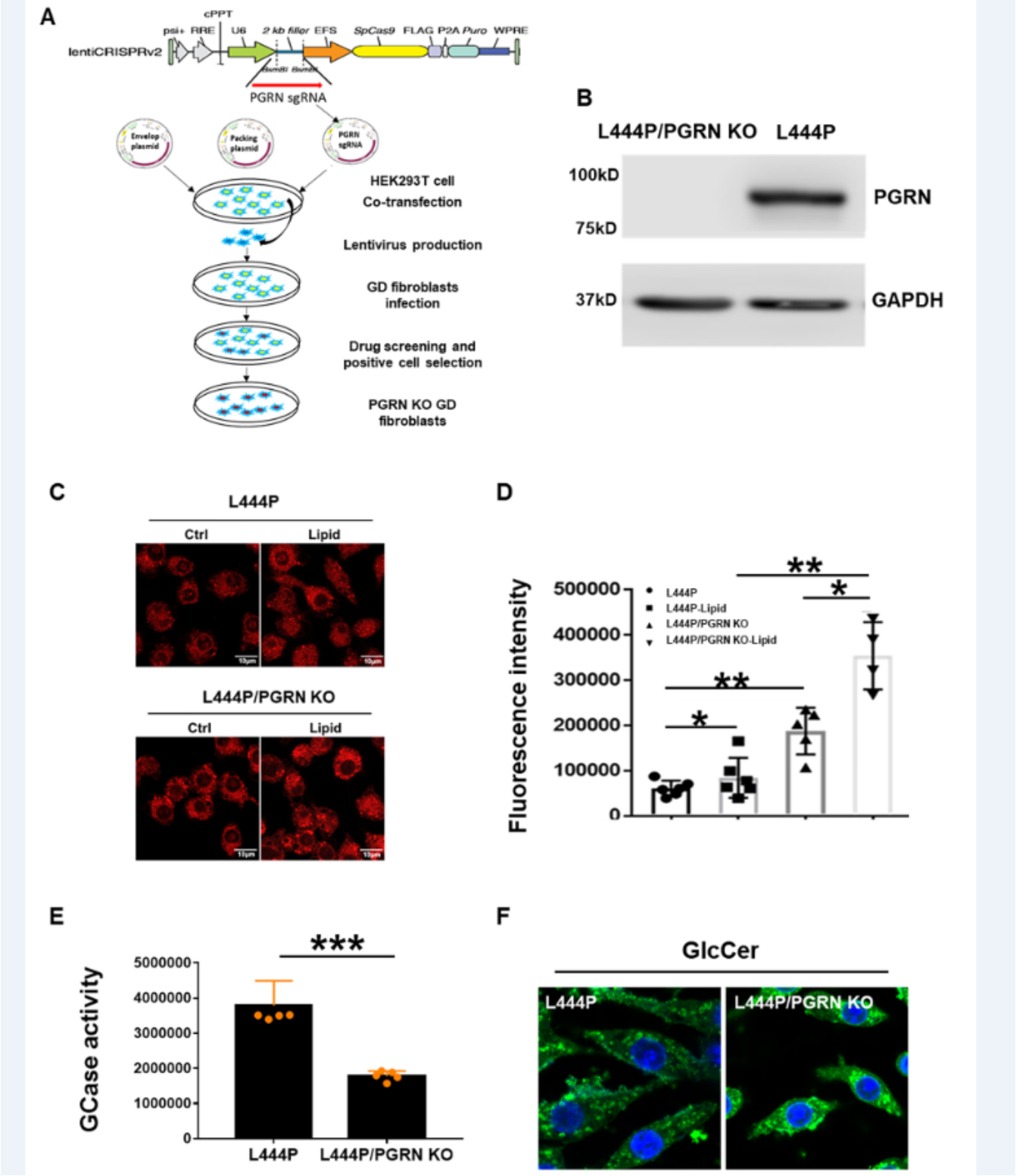

Figure 2

PGRN deficiency exacerbates the GD phenotype in GD patient fibroblasts. (A) A diagram of the CRISPR/Cas9 technique for construction of human PGRN-/- GD type 2 fibroblasts (L444P). (B) The levels of PGRN in PGRN KO (L444P/PGRN KO) and control L444P fibroblasts, assayed by Western blotting. (C) Live fluorescence microscopy imaging of LysoTracker Red staining in L444P and L444P/PGRN KO fibroblasts with or without lipid (50μg/ml) stimulation. (D) Quantification of the fluorescence intensity at

excitation/emission of 647/668 nm as shown in (C). (E) GCase activity in L444P and L444P/PGRN KO, assayed by released 4-methylumbelliferone. (F) The distribution of β-glucosylceramide (β-GlcCer, green) in L444P or L444P/PGRN KO fibroblasts. D and E, data are mean ± SD; * $p < 0.05$ or ** $p < 0.01$. (Scale bar, 5μm).

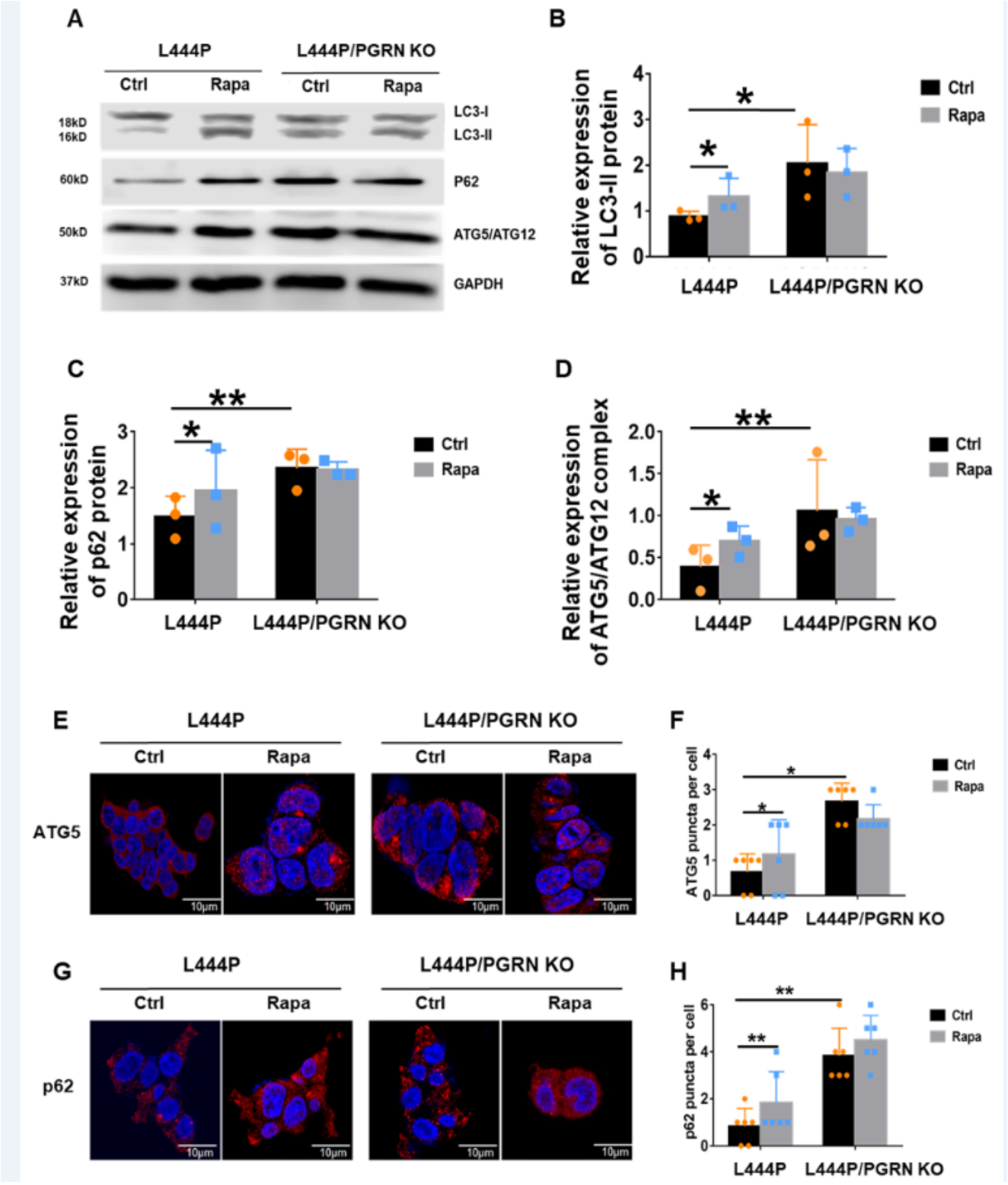

Figure 3

PGRN deficiency leads to autophagosome accumulation in GD fibroblasts. (A) Expression levels of autophagy markers LC3, p62, and ATG5/ATG12 complex in L444P or L444P/PGRN KO with rapamycin (100nM) stimulation, DMSO treatment used as an control. (B-D) Quantification of LC3-II (B), p62 (C), and ATG5/ATG12 complex (D) expression level. (E) ATG5 expression level in L444P or L444P/PGRN KO with or without rapamycin stimulation, assayed by immunofluorescence staining. (F) Quantification of E. (G) p62 expression level in L444P or L444P/PGRN KO with rapamycin stimulation or DMSO treatment, assayed by immunofluorescence staining. (H) Quantification of G. B, C, D, F and H, data are mean ± SD; * $p < 0.05$ or ** $p < 0.01$.

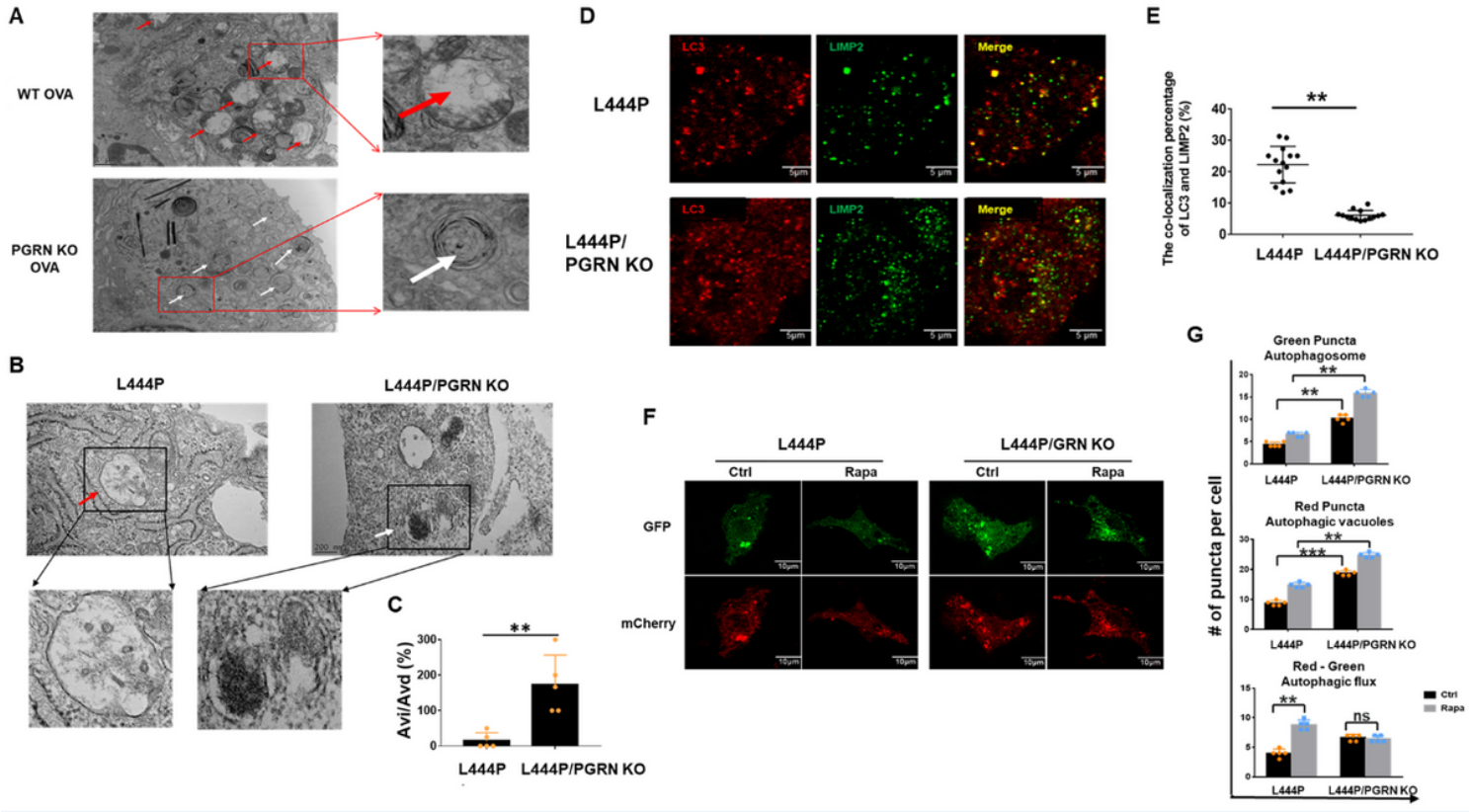

Figure 4

PGRN deficiency impairs the autophagosome-lysosome fusion. (A) Initial autophagic or degradative autophagic vacuoles in WT or PGRN KO mice with OVA challenge. Red arrows: Avd (Degradative autophagic vacuole), White arrows: Avi (Initial autophagic vacuole). (B) Ultrastructure of autophagic vacuoles in L444P or L444P/PGRN KO fibroblasts using transmission electron microscopy. Red arrows indicate degradative autophagic vacuole (Avd), white arrows indicate initial autophagic vacuole (Avi). (C) Quantification of the ratio of Avi to Avd in different cell groups. (D) Co-localization of LIMP2 and LC3 proteins in L444P or L444P/PGRN KO using confocal microscopy. Red staining: LC3, green staining: LIMP2, rapamycin; 100nM, 24 hours treatment. (E) Qualitative analysis of D. (F) Confocal microscopy

analysis of mCherry-GFP-LC3 in L444P or L444P/PGRN KO with or without rapamycin stimulation. MCherry+GFP− puncta indicates autolysosomes, mCherry+GFP+ (yellow) indicates autophagosome, they were both quantified and summarized in (G). C, E and G, data are mean ± SD; * p <0.05 or ** p < 0.01.

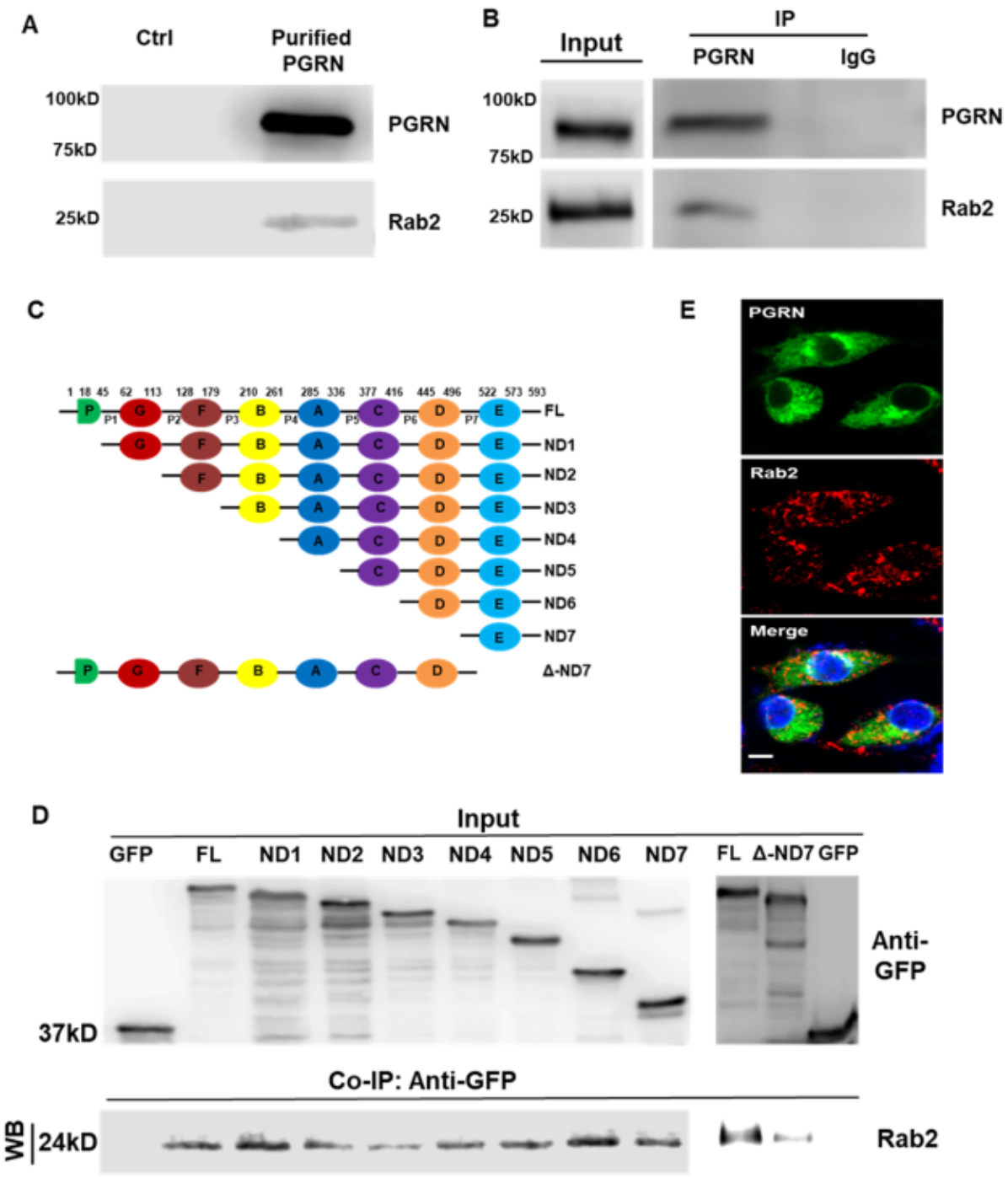

Figure 5

PGRN binds to Rab2 and Grn E is the major binding site. (A) Examination of the binding between PGRN and Rab2. Stable HEK293T cell lines expressing PGRN-His was established in our lab previously. PGRN-

His protein was purified from the PGRN-His-expressing HEK293T cells using HIS-Select Nickel Affinity Gel (Sigma-Alrich). The proteins co-purified with His-tagged PGRN were probed with Rab2 antibody. Cell lysate was used as control. (B) Co-IP assay to examine the binding between PGRN and Rab2 in GD patient fibroblasts. IgG used as a negative control. (C) Scheme of constructs encoding serial GFP-tagged full-length PGRN (aa 1-593) and N-terminal deletion mutants of PGRN: ND1 (aa45-593), ND2 (aa113-593), ND3 (aa 179-593), ND4 (aa 261-593), ND5 (aa 336-593), ND6 (aa 416-593), ND7 (aa 496-593), and Grn E deletion mutant Δ-ND7. (D) Co-IP assay. HEK293T cells were transfected with plasmids encoding GFP-fused full-length PGRN, or PGRN mutants as indicated, and the cell lysates were immunoprecipitated with GFP antibody. The complexes were probed with Rab2 antibody. GFP-fused vector was used as a negative control. (E) Co-localization of PGRN and Rab2 by confocal microscopy. The co-localization of PGRN and Rab2 was indicated by the white arrow in the merged image. Images were made at ×630 magnifications. (Scale bar, 5μm).

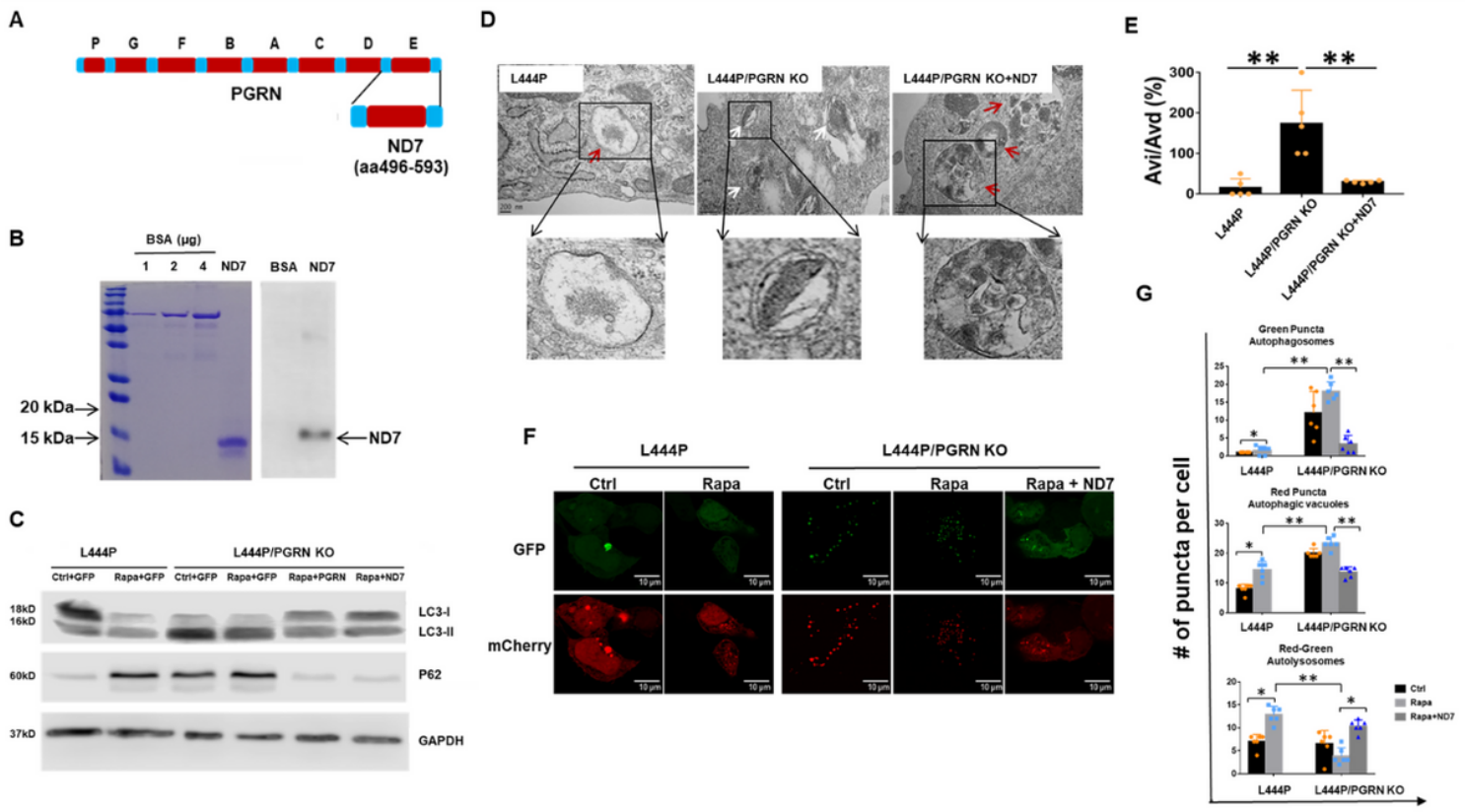

Figure 6

ND7 effectively ameliorates autophagy defects in PGRN deficient GD fibroblasts. (A) Structure of ND7. (B) Expression and characterization of recombinant ND7. Purified ND7 was analyzed by Coomassie blue staining (left) and western blotting with His antibody (right). (C) Effect of ND7 treatment on autophagic markers LC3-II and p62. L444P/PGRN KO were treated with ND7 recombinant protein (5μg/ml) for 24 hours. (D) Ultrastructure of autophagic vacuoles in L444P. L444P/PGRN KO were treated with ND7

recombinant protein (5μg/ml) for 24 hours and then the ultrastructure of the control L444P, L444P/PGRN KO, or L444P/PGRN KO + ND7, was observed under transmission electron microscopy. Red arrows indicate degradative autophagic vacuole (Avd), white arrows indicate initial autophagic vacuole (Avi). (E) Quantification of the ratio of Avi to Avd in different cell groups. (F) Confocal microscopy analysis of mCherry-GFP-LC3 in L444P or L444P/PGRN KO with or without recombinant ND7 (5μg/ml) administration in the absence or presence of rapamycin. MCherry+GFP− puncta indicates autolysosomes, mCherry+GFP+ (yellow) indicates autophagosome, they were both quantified and summarized in (G). E and G, data are mean ± SD; * $p < 0.05$ or ** $p < 0.01$.

Supplementary Files

This is a list of supplementary files associated with this preprint. Click to download.

- ZhaoXLetalSupplementarydata.docx.docx